High Strain Rate Superplasticity in an Al–Li–Mg Alloy Subjected to Equal-Channel Angular Extrusion

Fanil Musin[1,*], Rustam Kaibyshev[2], Yoshinobu Motohashi[1], Takaaki Sakuma[1] and Goroh Itoh[3]

[1]*Ibaraki University, Research Center for Superplasticity, Hitachi 316-8511, Japan*
[2]*Institute for Metals Superplasticity Problems, Khalturina 39, Ufa 450001, Russia*
[3]*Ibaraki University, Department of Mechanical Engineering, Hitachi 316-8511, Japan*

The superplastic behavior of an Al–4.1%Mg–2.0%Li–0.16%Sc–0.07%Zr alloy (1421 Al) subjected to intense plastic straining by equal-channel angular extrusion (ECAE) was studied in the temperature interval 250–450°C at strain rates ranging from 1.4×10^{-5} to $1.4\,s^{-1}$. The grain size after ECAE was about 0.8 μm and the fraction of high angle boundaries was about 80 pct. The highest elongation of 1850% without failure appeared at a temperature of 400°C and initial strain rate of $1.4 \times 10^{-2}\,s^{-1}$ with corresponding coefficient of the strain rate sensitivity of 0.6. It was shown that the ECAE processed 1421 Al exhibits superior superplastic properties in the temperature range 300–450°C with the strain rate sensitivity higher than 0.4. Microstructural evolution and cavitation during high strain rate superplastic deformation were examined.

Keywords: *high strain rate superplasticity, aluminum alloys, microstructural evolution, equal-channel angular extrusion, strain hardening*

1. Introduction

There is now a great interest in developing new Al–Li–Mg alloys, which are promising materials for aerospace applications due to excellent combination of high strength and light weight.[1)] However, these alloys are characterized by low workability. It has been shown that it is possible to improve their formability as well as service properties by making these alloys superplastic.[2)] Superplastic deformation was used to produce components with complex shapes from an Al–Li–Mg–Zr alloy.[2)] However, the utilization of this technology in commercial scale is currently limited because of the relatively low strain rates associated with superplastic deformation[2,3)] and difficulties in producing ultra-fine grain structure in Al–Li–Mg alloys using standard procedures associated with thermomechanical processing.[2)]

The development of new superplastic aluminum alloys produced by ingot metallurgy and containing additions of Zr and/or Sc, through recent advances in grain refinement via intense plastic straining, has led to a new area of high strain rate superplasticity (HSRS).[4–6)] Ultrafine grain sizes introduced by equal-channel angular extrusion (ECAE) in these alloys are retained at elevated temperatures owing to nanoscale $Al_3(Zr, Sc)$ particles. Experiments on an Al–Li–Mg–Zr alloy designated as 1420 aluminum alloy (1420 Al) have shown that superior superplastic properties may be achieved at high strain rates and low temperatures after ECAE.[6–10)]

Recently, a new Al–Li–Mg–Zr alloy designated as 1421 aluminum alloy (1421 Al) containing Sc and decreased amounts of alloying additions of Li and Mg has been developed.[1)] The 1421 Al exhibits enhanced service properties and improved formability.[1)] However, to date, there exist no systematic data on superplastic behavior of this material. The present study was initiated to evaluate superplastic properties of the 1421 Al subjected to ECAE. Moreover, a specific objective of this work is to examine the microstructural evolution and cavitation during high-strain-rate superplastic deformation.

2. Material and Experimental Procedure

The material used in the present study was a commercial grade version of the 1421 Al. The composition of the alloy is given in Table 1. The alloy was manufactured by direct chill casting followed by solution treatment at 460°C for 24 h. Then the 1421 Al was finally cut into cylinders with 20 mm in diameter and 100 mm in length. The ECAE was conducted using an isothermal die with a circular internal cross-section. The channel had an L-shaped configuration with angles ϕ and ψ (as defined by Iwahashi *et al.*[11)]) both equal to 90°. The diameter of this channel was 20 mm. Deformation through these angles produces a strain of ~ 1 on each passage through the die. The pressing speed was ~ 10 mm/s. The rods were repetitively pressed through the die at 325°C to a total strain of ~ 16, and the samples were rotated by 90° in the same sense between each pressing in the procedure designated as route B_C.[12)]

Tensile specimens were cut parallel to the longitudinal axes of the pressed rods with a gauge length of 6 mm and cross-section of $1.5 \times 3\,mm^2$. These samples were deformed in tension to failure in air using a Shimadzu universal testing machine (Model AG-G-20kN) operating at a constant crosshead speed. Tension tests were carried out in the temperature interval 250–450°C at strain rates ranging from 1.4×10^{-5} to $1.4\,s^{-1}$. Temperature fluctuation was within ±2°C. Each

Table 1 Composition of the 1421 Al determined from chemical analysis (in wt.%).

Mg	Li	Sc	Zr	Si	Fe	Al
4.1	2.0	0.16	0.07	0.07	0.08	Bal.

*Corresponding author: E-mail: musin@ipc.ibaraki.ac.jp, On leave from Institute for Metals Superplasticity Problems, Ufa, Russia.

sample was heated to the testing temperature over a period of about 30 min and then was held at this temperature for about 30 min in order to reach thermal equilibrium. The values of the strain rate sensitivity ($m = d\ln\sigma/d\ln\dot{\varepsilon}$, where σ is flow stress, $\dot{\varepsilon}$ is strain rate) were determined by strain-rate-jump tests.[2,3]

Samples for metallographic examinations were annealed at 170°C for 4 h in order to decorate grain boundaries with secondary phase particles. These grain-boundary particles were revealed by etching with standard Keller's reagent. Metallographic analysis was carried out using an Olympus BX60 optical microscope. The mean grain size was determined by the linear intersect method from measurements of more than 300 grains in longitudinal and transverse directions. Cavitation was measured in samples pulled to failure by optical microscopy using the standard point-count technique. Areas located 3 mm from the fracture surface were analyzed.

For TEM examinations, samples were ground to about 0.2 mm in thickness. Discs with 3 mm diameter were cut and electropolished to perforation with a Tenupol-3 twinjet polishing unit using a 30% nitric acid solution in methanol at −30°C and 15 V. A Jeol JEM-2000EX electron microscope with a double-tilt stage at an accelerating voltage of 200 kV was used for the thin foil examinations. Misorientations of the grain boundaries induced by the ECAE were analyzed using the conventional Kikuchi-line technique. The accuracy of measurements was about 1°. Misorientation analysis was applied to about 50 grain boundaries.

3. Results and Discussion

3.1 Microstructure after ECAE

The microstructure of 1421 Al in as-cast state after solution treatment consisted of uniform equiaxed grains with an average grain size of about 60 μm. Second-phase particles were identified by the TEM analysis as Al_2LiMg (designated as S-phase) and Al_3Sc/Zr.

A typical microstructure of the 1421 Al processed by ECAE and the corresponding misorientation map are presented in Fig. 1(a). It is clearly seen that the ECAE processing at 325°C to a strain of 16 resulted in the formation of fine crystallites with an average size of about 0.8 μm. High-angle boundaries, which were thought to be over 15°,[13] account for ~80% of deformation-induced boundaries and, therefore, high-angle boundaries dominate in the resulted structure.

The careful observation of many areas showed that microstructure of the ECAE processed 1421 Al is reasonably homogeneous on a macroscopic level, although stringers of secondary phase, mainly S-phase, can be revealed by etching as stringers of dark pits (Fig. 1(b)). These stringers aligned along prior extrusion direction. It should be noted that elongated unrecrystallized areas containing recovered subgrains were rarely observed.

Notably, the resulted grain size after ECAE in the 1421 Al (~0.8 μm) is less than that (~1.2 μm) attained in the 1420 Al pressed finally at 200°C.[6–10]

3.2 Mechanical properties

The true stress-true strain curves (σ-ε) for the ECAE processed 1421 Al at two fixed temperatures (300 and 400°C)

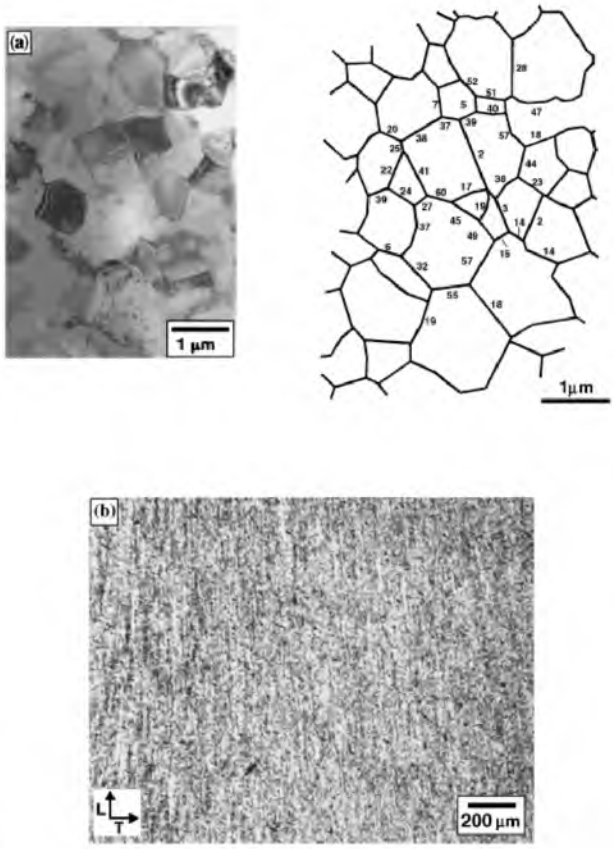

Fig. 1 Typical ultrafine-grained structure in 1421 Al deformed to a strain of about 16 via ECAE at 325°C: (a) TEM, (b) macrostructure. The misorientation map represents the misorientations of deformation-induced boundaries in degree. Arrows indicate the tension (L) and long-transverse (T) directions.

and strain rates ranging from 1.4×10^{-3} to $1.4\,s^{-1}$ are depicted in Figs. 2(a) and (b), respectively. Figure 2(c) shows the σ-ε curves obtained at an initial strain rate of $1.4\times10^{-2}\,s^{-1}$ over a range of temperatures. Strain hardening takes place in a beginning stage of the deformation. After reaching the peak stress, the stress continuously decreases until fracture. Increasing strain rate or decreasing temperature leads to a shift of the peak stress to a lower strain and the increase in strain-hardening rate. The relationship between the peak strain, ε_p, at which the peak stress, σ_p, appears, and this peak stress is shown in Fig. 3. It is seen that ε_p value tends to decrease gradually with increasing σ_p. In the range of temperatures and strain rates, at which elongation exceeded 1000% ($\varepsilon > 2.4$), the peak strain was about 1.0. A well-defined peak in flow stress is observed at lower temperatures and higher strain rates, at which an evidence for localization of plastic deformation resulting in the final necking and fracture was observed. At $T \geq 350$°C and $\dot{\varepsilon} = 1.4\times10^{-2}\,s^{-1}$, apparent steady-state flow can be distinguished, and the very uniform deformation within the gauge length occurs as seen in Fig. 4. As a result, the samples exhibit exceptionally high tensile ductilities. At 400°C, the ductility was so high that the specimen remained unbroken even after 1850% elongation.

A weak strain dependence of the m value is seen in Fig. 5. At 400°C and $\dot{\varepsilon} = 1.4\times10^{-2}\,s^{-1}$, the m value slightly increases with strain at $\varepsilon \leq \varepsilon_p$. Subsequent deformation results in gradual decrease in the m value.

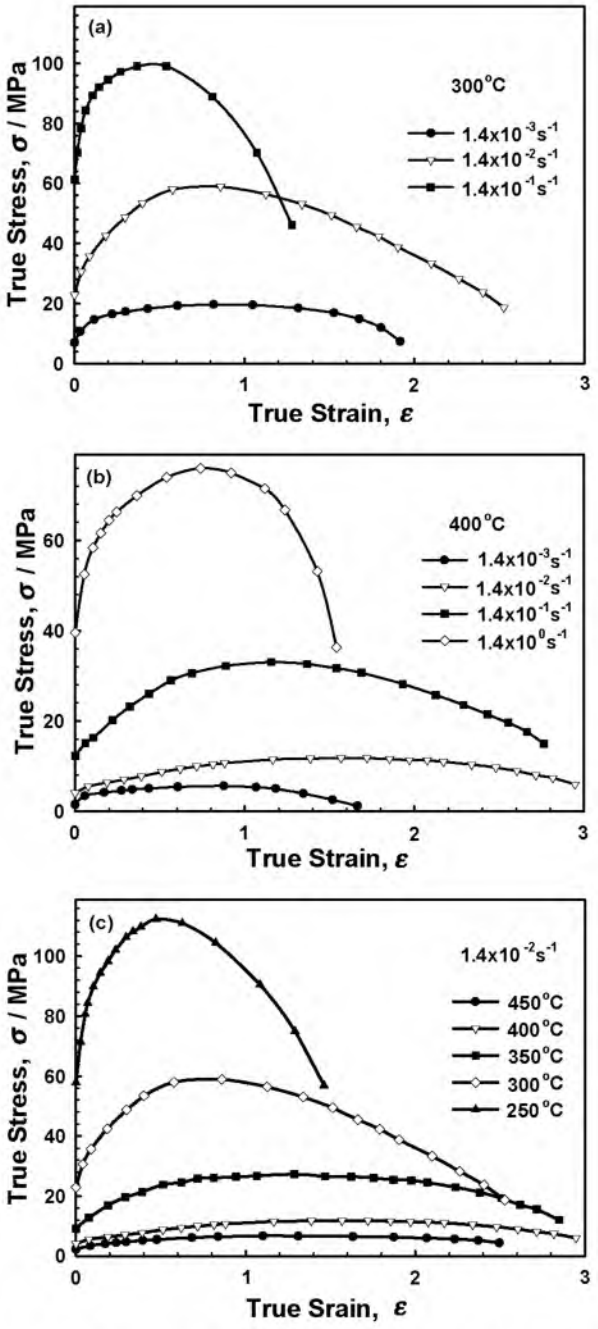

Fig. 2 Effect of strain rate on true stress-true strain curves for the 1421Al alloy subjected to ECAE. (a) 300°C; (b) 400°C. Effect of temperature on σ-ε curves at an initial strain rate of $1.4 \times 10^{-2}\,s^{-1}$ (c).

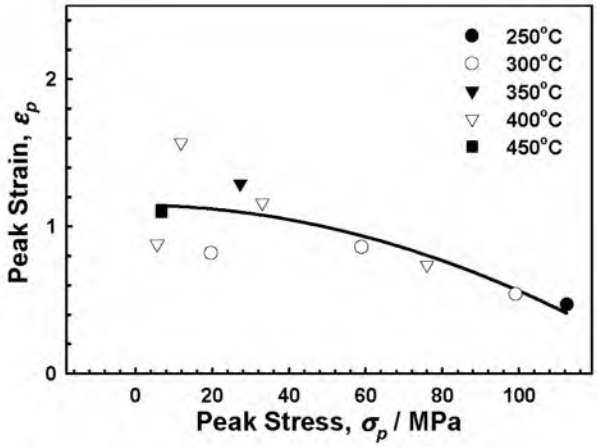

Fig. 3 Relationship between peak strain, ε_p, and peak stress, σ_p.

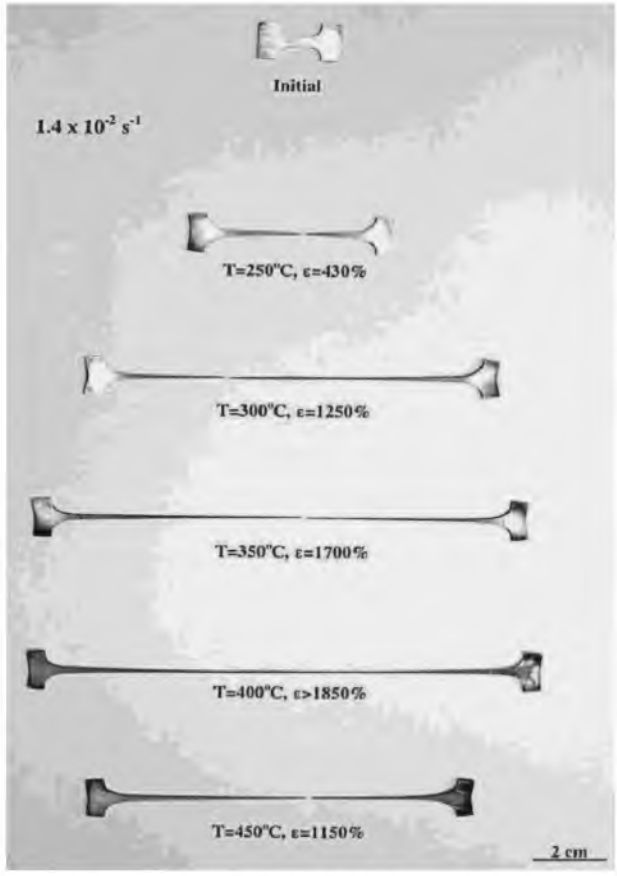

Fig. 4 The samples of the 1421Al after ECAE processing and pulling to failure at different temperatures and $\dot{\varepsilon} = 1.4 \times 10^{-2}\,s^{-1}$.

It is well known that stability of plastic flow resulting in uniform deformation depends on the strain hardening coefficient, θ, as well as the m value.[14] The strain hardening was evaluated as the ratio of the peak stress to the yield stress (σ_p/σ_y). Effect of strain rate on the θ value is shown in Fig. 6(a). The variation in the strain hardening coefficient with temperature is depicted in Fig. 6(b). It is seen that decreasing the strain rate and increasing the temperature led to increase in the θ value. In the range where high superplastic elongation (> 1000%) appeared, the strain hardening is higher than 3 providing very uniform plastic flow at strains less than ε_p. Thus, uniform tensile deformation shown in Fig. 4 is provided by a combination of high values of the strain rate sensitivity with superior strain hardening at $\varepsilon < \varepsilon_p$. Therefore, there is an advanced possibility to keep uniform superplastic deformation in the ECAE processed 1421 Al at strains less than 1.0, that can be used for metal working of complex parts requiring deep drawing and high blow forming capacities.

Flow stresses, σ, taken at a true strain of ~ 0.4, elongation-to-failure δ and the coefficient m are plotted in Fig. 7 as a function of strain rate in double logarithmic scale. Three regions of superplastic deformation[2,3] can be distinctly distinguished. A sigmoidal relationship between flow stress and strain rate, which is typical for superplastic behavior, is seen (Fig. 7(a)). The highest values of the coefficient m and δ are found at a strain rate of $1.4 \times 10^{-2}\,s^{-1}$ (Figs. 7(b) and (c)).

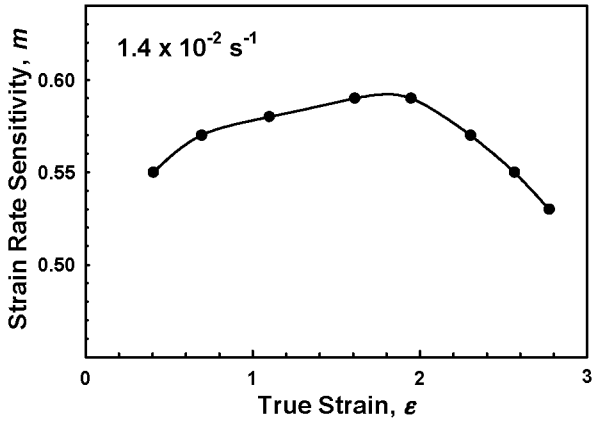

Fig. 5 The effect of strain on the coefficient of strain rate sensitivity, m, at 400°C and $\dot{\varepsilon} = 1.4 \times 10^{-2}\,s^{-1}$.

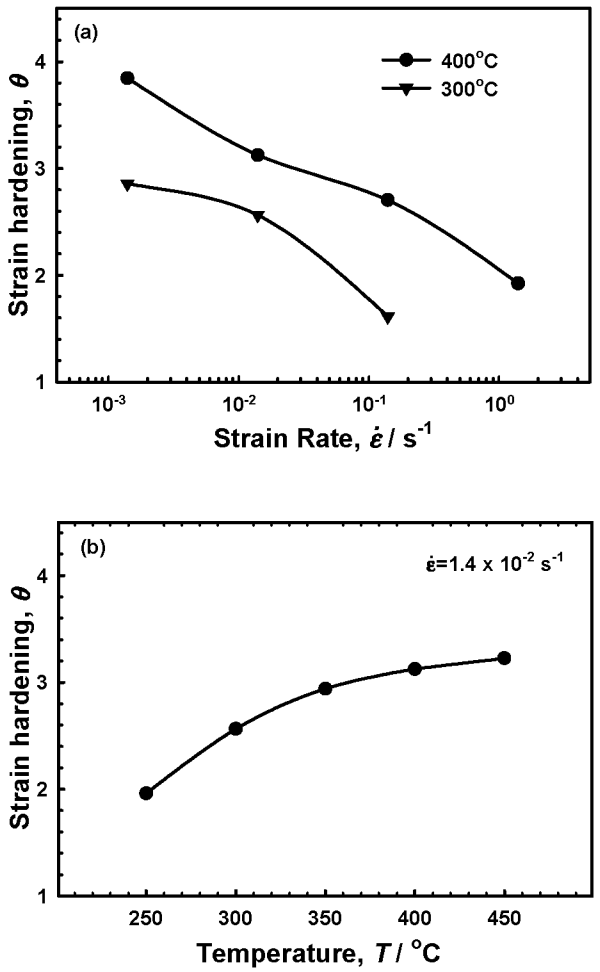

Fig. 6 The effects of temperature (a) and strain rate (b) on the strain hardening, θ.

The test denoted with the vertical arrow in Fig. 7(b) was discontinued without failure. The optimal strain rate region (*i.e.* region 2) for superplasticity, in which $m \geq 0.33$, expands from 1.4×10^{-3}–$8 \times 10^{-2}\,s^{-1}$ at 300°C to 1.4×10^{-3}–$1.4\,s^{-1}$ at 400°C. Therefore, the optimal region tends to expand to higher strain rates with increasing temperature.

Temperature dependencies of the coefficient m and δ at $\dot{\varepsilon} = 1.4 \times 10^{-2}\,s^{-1}$ are plotted in Fig. 8. Increase in temperature from 250 to 400°C leads to increase in the m value from 0.38

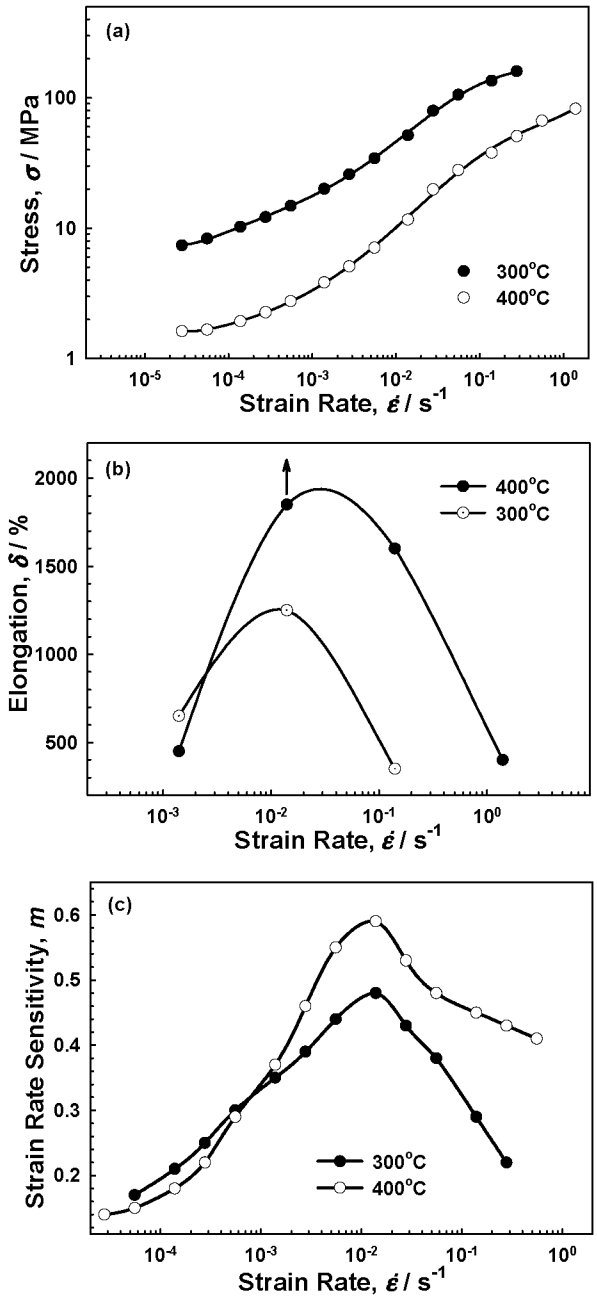

Fig. 7 (a) Flow stress, σ, taken at $\varepsilon \sim 0.4$; (b) elongation-to-failure, δ; and (c) the coefficient of strain rate sensitivity, m, as a function of strain rate.

to 0.6 and the δ value from 430% to > 1850%. Further raising of the temperature to 450°C results the coefficient m and the tensile elongation in decrease.

Notably, the ECAE processed 1421 Al exhibits ductility higher than ~430% at all temperatures and strain rates examined. Thus, this aluminum alloy behaves as a typical superplastic material at high strain rates in the very wide range of temperatures.

3.3 Microstructural evolution

The microstructural evolution of the 1421Al was examined under conditions of static annealing in grip sections (Fig. 9) and superplastic deformation, *i.e.* dynamic annealing in the gauge section, (Fig. 10) in the temperature range of 250–450°C at $\dot{\varepsilon} = 1.4 \times 10^{-2}\,s^{-1}$. Grain sizes observed after static

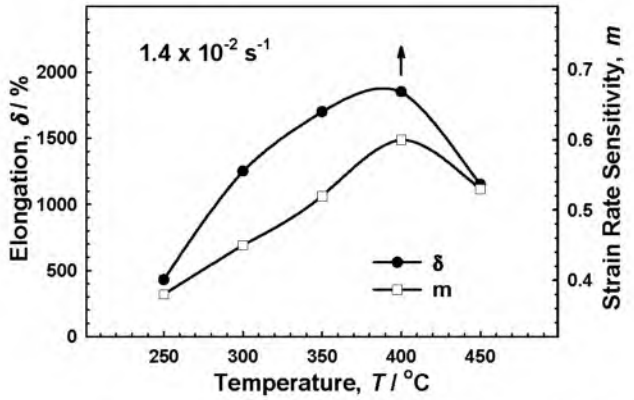

Fig. 8 The coefficient of strain rate sensitivity, m, and elongation-to-failure, δ, as a function of temperature.

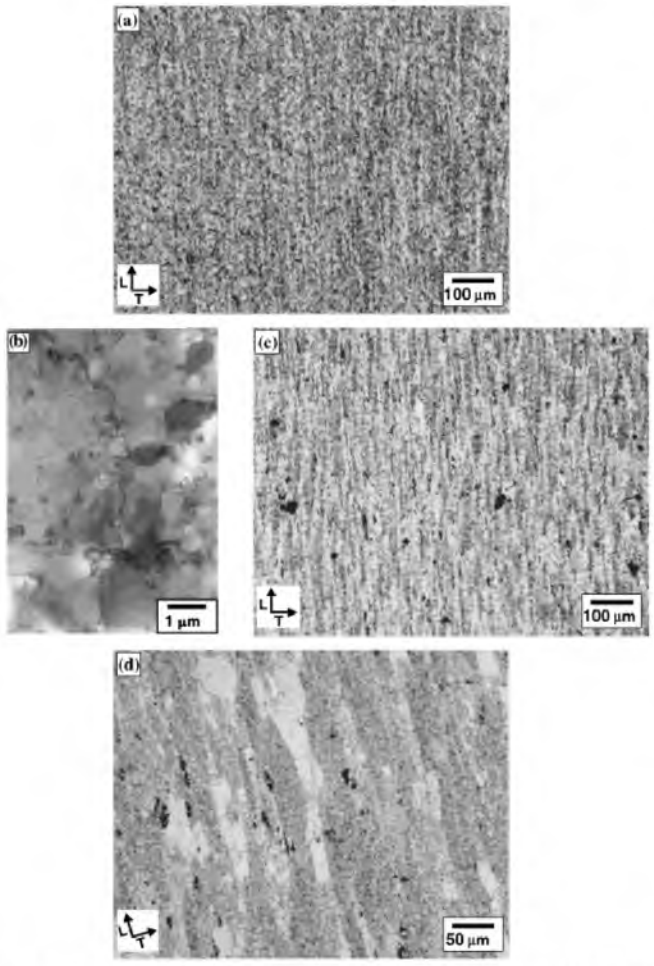

Fig. 9 Effect of static annealing on structures developed by ECAE at: (a) 350°C, (b, c) 400°C and (d) 450°C. Arrows indicate the tension (L) and long-transverse (T) directions.

annealing (L_s), dynamic annealing (L_d) and grain aspect ratio (AR) are summarised in Table 2.

It is seen that the initial grain size remains essentially stable under static annealing at $T \leq 350$°C (Fig. 9(a)). Onset of the grain growth can be detected in grip section only at 400°C (Fig. 9(b)). However, recrystallized matrix at this temperature is essentially stable (Fig. 9(c)). Grain growth takes place only within unrecrystallized areas, which are highly elongated along former extrusion directions. It is apparent

Table 2 Average grain sizes after static annealing, L_s, and superplastic deformation, L_d, for the samples pulled to failure at a strain rate of 1.4×10^{-2} s^{-1} and different temperatures. The strain in the gauge section and the time of static annealing in the grip section (in hours) are also indicated.

	350°C (1700%, 0.87 h)	400°C (1850%, 0.9 h)	450°C (1150%, 0.75 h)
L_s, μm	0.9	1.2	2.3
L_d, μm*	2.7/2.3	3.9/3.2	7.1/4.7
AR	1.21	1.22	1.51

*Numerator and denominator are grain sizes measured in the longitudinal and transverse directions, respectively.

that this abnormal static growth is attributed to the extensive growth of initially elongated unrecrystallized areas by a mechanism which is similar to that termed as "recrystallization *in situ*".[15] It is worth noting that the grain size after static annealing in the present 1421 Al (Table 2) is less than that in the 1420 Al.[6,8,10,16]

At 450°C, a mixed structure consisting of two structural components was revealed in grip section (Fig. 9(d)). One of the components is recrystallized grains with an average size of about 2 μm exhibiting equiaxed shape. Volume fraction of these grains is about 70 pct. The other structural component is the highly elongated grains with an average size of ~ 64 μm along the former extrusion direction. Their average size in the transverse direction is ~ 18 μm. Volume fraction of these grains is about 30 pct. It is apparent that inclusion of S-phase locating along former extrusion direction as planar arrays can effectively pin migrating grain boundaries in transverse direction.[17] Concurrently, the curved boundary does not experience any pinning in longitudinal direction lying parallel to chains of S-phase.[17] As a result, the anisotropy in distribution in S-phase is reflected in the shape of grains[17] which highly elongate along former extrusion direction with increasing temperature from 400 to 450°C.

Superplastic deformation leads to remarkable grain growth (Table 2, Fig. 10). However, the grain size remains less than 4 μm even after 1850% elongation at 400°C and 1.4×10^{-2} s^{-1} (Fig. 10(b)). It is apparent that the weak strain dependence of m value is caused by low rate of dynamic grain growth. It is worth noting that the resulted structure is uniform, suggesting occurrence of dynamic recrystallization resulted in the grain refinement within the elongated unrecrystallized areas during superplastic deformation.

Superplastic deformation causes slight grain elongation along the tension axis (Fig. 10) and grain aspect ratio, defined as the ratio of the grain dimension in the longitudinal direction to that in the transverse direction, tends to increase with increasing temperature (Table 2) In the temperature range of 350–400°C, the grain aspect ratio is about 1.2. This value is typical for conventional superplastic alloys, where the high contributions of grain boundary sliding (GBS) to the total elongation take place.[2,3] Raising of the temperature up to 450°C leads to the increase in the grain aspect ratio to 1.5 (Table 2). In general, relatively high grain aspect ratio after superplastic deformation is attributed to increased contribution of dislocation glide to total deformation.[2,3]

Examination of porosity at a strain rate of 1.4×10^{-2} s^{-1}

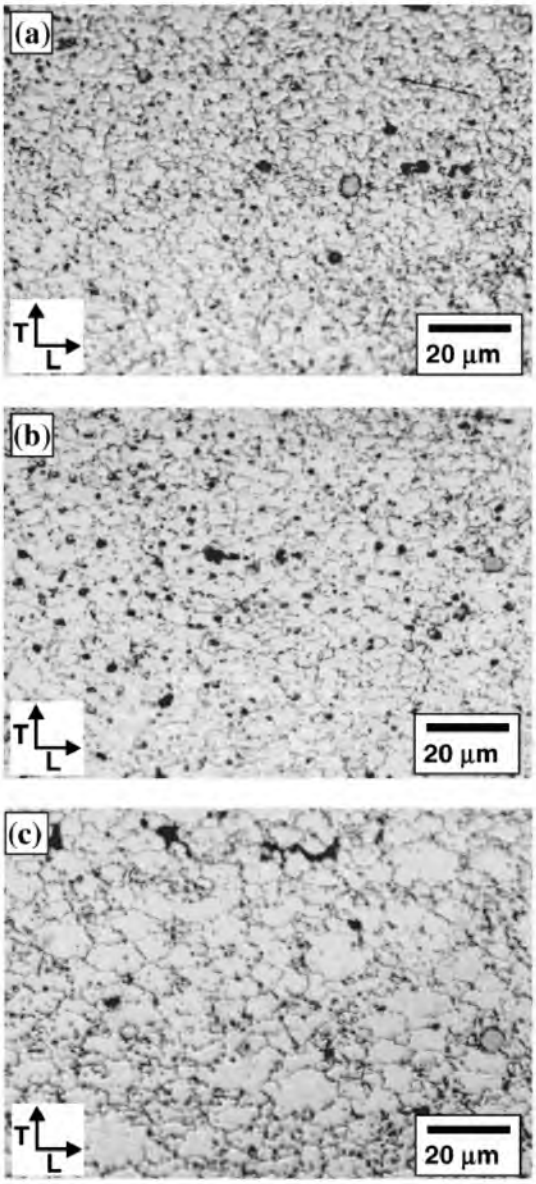

Fig. 10 Microstructure evolved after superplastic deformation at $\dot{\varepsilon} = 1.4 \times 10^{-2}\,s^{-1}$. (a) 350°C, $\varepsilon = 2.8$; (b) 400°C, $\varepsilon = 3$ and (c) 450°C, $\varepsilon = 2.5$. Arrows indicate the tension (L) and long-transverse (T) directions.

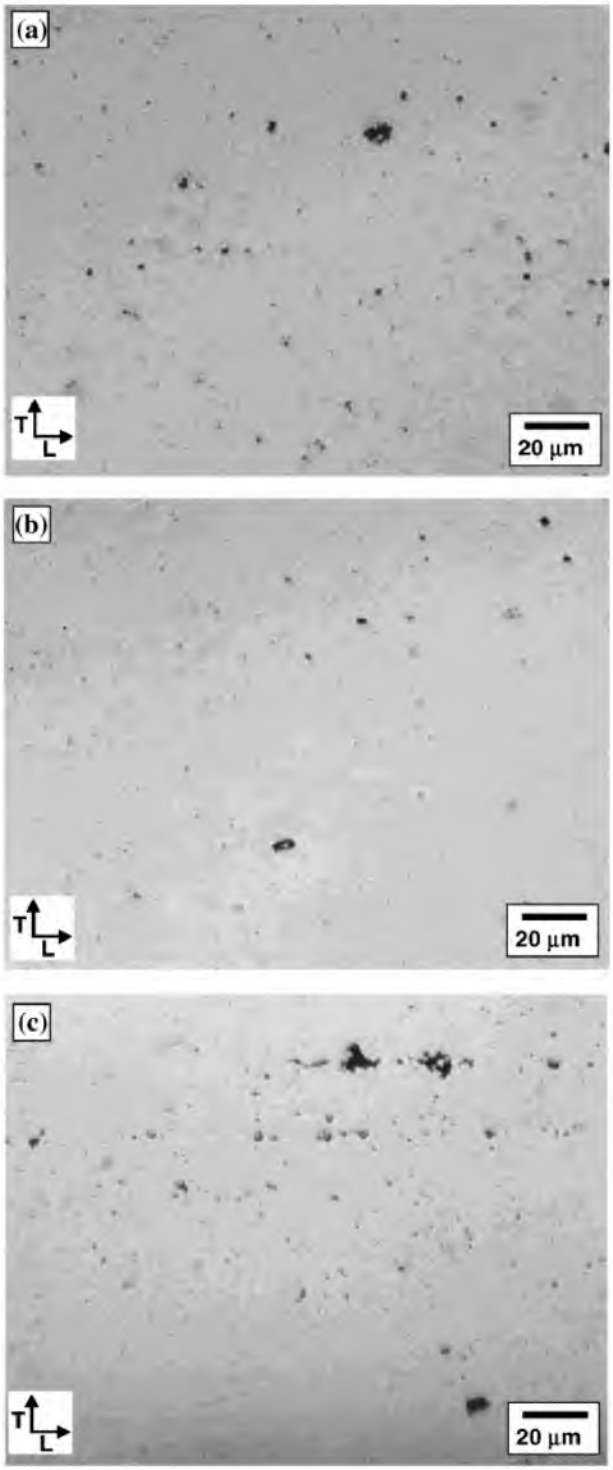

Fig. 11 Cross-sectional view of samples strained at $\dot{\varepsilon} = 1.4 \times 10^{-2}\,s^{-1}$. Micrographs were taken in places 3 mm from the fracture surface. Arrows indicate the tension (L) and long-transverse (T) directions. (a) 350°C $\varepsilon = 2.8$; (b) 400°C, $\varepsilon = 3$ and (c) 450°C, $\varepsilon = 2.5$.

and different temperatures shows that in the temperature range 250–400°C the 1421Al exhibits limited cavitation (Fig. 11). For example, in the 1421 Al strained to 1850% at 400°C without failure, the volume fraction of cavities is negligible ($\sim 0.3\%$). It is pointed out that most of the dark phases in Fig. 11(b) might be, in fact, impure inclusions.

Figure 12 shows cross-sectional views from four consecutive areas in a sample deformed to 1650% at 400°C and $1.4 \times 10^{-1}\,s^{-1}$. It is clearly seen that almost no remarkable cavitation takes place both close to the fracture surface and at a distance of ~ 1 mm from this surface. Near the fracture tip, shown in Fig. 10, an evidence for the development of intergranular cracking can be found. These cracks form along the tensile direction.

At 450°C, increased cavitation (cavity volume fraction is $\sim 2\%$) is observed (Fig. 11(c)). Two types of cavities can be distinguished. One of them is the fine equiaxed cavities evolved by diffusion-controlled cavity growth. In addition, cavities exhibiting irregular and jagged shape were found. Most of large cavities align in the tensile direction and form stringers. These large cavities developed by plasticity-controlled cavity growth mechanism suggest that the cavitation is a result of extensive and non-uniform GBS.[18] This observation suggests a plasticity-controlled cavity growth mechanism, indicating cavitation is a result of extensive and non-

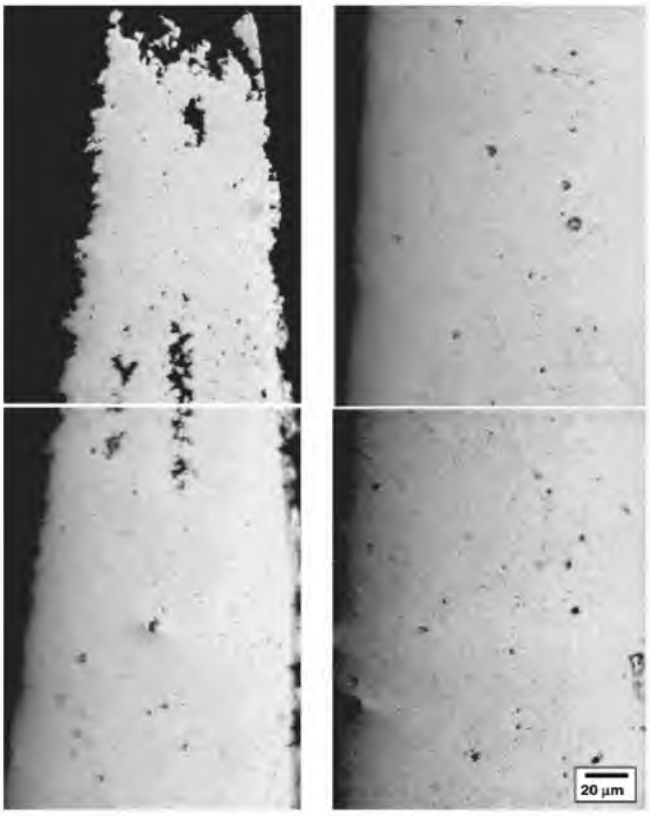

Fig. 12 Cross-sectional views from four consecutive areas in sample deformed to 1650% at 400°C and $1.4 \times 10^{-1}\ s^{-1}$.

uniform GBS.[13] Notably, even at 450°C, cavitation is significantly less than other superplastic aluminum alloys.[3]

3.4 Effect of Sc addition on high strain rate superplasticity in the Al–Li–Mg alloy

Let us summarize the present data for 1421 Al comparing with those obtained for the 1420 Al.[6–10,16] The present study demonstrated the feasibility of achieving excellent superplastic properties in the commercial 1421 Al, which are higher than those in the 1420 Al subjected to the essentially similar processing. It has been established that ECAE at 325°C to a strain of 16 is an attractive way to introduce equiaxed and ultrafine grains in the 1421 Al which becomes capable for high strain rate superplasticity. At 400°C, the highest elongations achieved were 1850 and 1700% at initial strain rates of 1.4×10^{-2} and $1.4 \times 10^{-1}\ s^{-1}$, respectively. On the other hand, the highest elongations in the 1420 Al were achieved 1180% and 1210% at the same deformation conditions.[6,8,10]

Superior superplastic properties in the 1421 Al subjected to ECAE can be attributed to the presence of coherent $Al_3(Sc, Zr)$ dispersoids, which are highly effective in pinning of deformation induced boundaries of ultrafine grains with a size less than 1 μm at temperatures below 400°C. Therefore, the modification of chemical composition of the 1420 Al provided increases in both service properties[1] and workability as well. The latter is associated with the fact that the addition of Sc are more effective than Zr addition in inhibiting grain growth at elevated temperatures in Al–Li–Mg alloys. This is the reason why the grain size after static annealing in the present alloy is smaller than that in the 1420 Al,[6,8,10,16] and ultra-fine grain structure in the 1421 Al exhibits increased stability under superplastic deformation.

The other important observation in the present study is the fact that the 1421 Al after ECAE processing is not susceptible to cavitation in the temperature interval 250–400°C due to fine grain size facilitating accommodation of the GBS;[2,3] fracture occurs mainly due to crack propagation. It should be noted that the same result was revealed in the 1420 Al at 400°C.[6,10]

Therefore, degradation of service properties due to cavitation hardly takes place during superplastic deformation of the 1421 subjected to ECAE.

4. Conclusions

(1) Ultrafine grain size of about 0.8 μm was obtained in the as-cast commercial grade 1421 aluminum alloy (Al–Mg–Li–Sc) subjected to ECAE pressing at 325°C to a true strain of 16.

(2) High strain rate superplasticity was achieved in this alloy in the temperature interval 250–450°C. High tensile elongations (> 1000%) were found at temperatures ranging from 300 to 450°C and strain rates ranging from 1.4×10^{-2} to $1.4 \times 10^{-1}\ s^{-1}$. The highest total elongation without failure (≥ 1850%) with corresponding strain rate sensitivity of 0.6 was recorded at 400°C and initial strain rate of $1.4 \times 10^{-2}\ s^{-1}$.

(3) The ECAE processed 1421 Al exhibited high strain hardening ($\theta \sim 3$) in the temperature range 250–450°C.

(4) Ultrafine grained structure produced by ECAE showed high stability under both static and dynamic conditions at ≤ 400°C.

(5) The 1421 Al subjected to ECAE was not susceptible to cavitation in the temperature interval 250–400°C and the fracture occurred mainly owing to crack propagation.

Acknowledgements

We thank Mr. D. Gromov for his assistance with the ECAE processing. The financial support by the International Science and Technology Centre under Project no. 2011 and Light Metal Educational Foundation are gratefully acknowledged.

REFERENCES

1) I. N. Fridlyander: Met. Sci. Heat Treat. **1** (2001) 5–9.
2) O. A. Kaibyshev: *Superplasticity of Alloys, Intermetallides, and Ceramics*, (SpringerVerlag, Berlin, 1992) pp. 316.
3) T. G. Nieh, J. Wadsworth and O. D. Sherby: *Superplastisity in Metals and Ceramics*, (Cambridge University Press, New York, 1996) pp. 210.
4) Z. Horita, M. Furukawa, M. Nemoto, A. G. Barnes and T. G. Langdon: Acta Mater. **48** (2000) 3633–3640.
5) S. Komura, Z. Horita, M. Furukawa, M. Nemoto and T. G. Langdon: Metall. Mater. Trans. **32A** (2001) 707–716.
6) S. Lee, P. B. Berbon, M. Furukawa, Z. Horita, M. Nemoto, N. K. Tsenev, R. Z. Valiev and T. G. Langdon: Mater. Sci. Eng. **A272** (1999) 63–72.
7) R. Z. Valiev, DA. Salimonenko, N. K. Tsenev, P. B. Berbon and T. G. Langdon: Scr. Mater., **37** (1997) 1945–1950.
8) P. B. Berbon, N. K. Tsenev, R. Z. Valiev, M. Furukawa, Z. Horita, M. Nemoto and T. G. Langdon: Metall. Trans. A **29A** (1998) 2237–2243.
9) P. B. Berbon, M. Furukawa, Z. Horita, M. Nemoto, N. K. Tsenev, R. Z. Valiev and T. G. Langdon: Philos. Mag. Lett. **78** (1998) 313–318.
10) M. Furukawa, Z. Horita, M. Nemoto and T. G. Langdon: Mater. Sci. Tech. **16** (2000) 1330–1333.
11) Y. Iwahashi, Z. Horita, M. Nemoto and T. G. Langdon: Acta Mater. **45**

(1997) 4733–4741.
12) M. Furukawa, Y. Iwahashi, Z. Horita, M. Nemoto and T. G. Langdon: Mater. Sci. Eng. **A257** (1998) 328–332.
13) J. P. Hirth and J. Lothe: *Theory of dislocations*, (McGraw-Hill Book Company, New York, 1968) p. 598.
14) B. Ash and C. H. Hamilton: *Superplasticity and Superplastic Forming*, C. H. Hamilton and N. E. Paton, eds., (The Minerals, Metals and Materials Society, 1988) 239–244.
15) F. Haeßner: *Recrystallization of metallic materials*, (Dr. Riederer Verlag GbmH, Stuttgart, 1978) p. 336.
16) F. J. Humphreys and M. Hatherly: *Recrystallization and Related Annealing Phenomena*, (Pergamon Press, Oxford, 1996) p. 497.
17) M. Furukawa, Y. Iwahashi, Z. Horita, M. Nemoto, N. Tsenev, R. Valiev and T. G. Langdon: Acta Mater. **45** (1997) 4751–4757.
18) M. G. Zelin, N. A. Krasilnikov, R. Z. Valiev, M. W. Grabski, H. S. Yang and A. K. Mukherjee: Acta Metall. Mater. **42** (1994) 119–131.